ACS APPLIED MATERIALS & INTERFACES

Research Article

www.acsami.org

Toward Anisotropic Materials via Forced Assembly Coextrusion

Tiffani M. Burt, Alex M. Jordan, and LaShanda T. J. Korley*

Department of Macromolecular Science and Engineering, and Center for Layered Polymeric Systems, Case Western Reserve University, Cleveland, Ohio 44106-7202, United States

Supporting Information

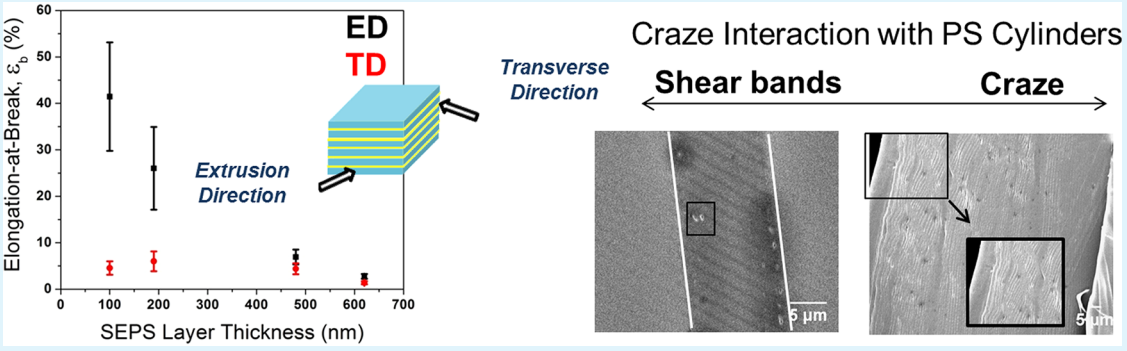

ABSTRACT: Multilayer coextrusion offers a diverse platform to examine layer dependent confinement effects on self-assembling nanomaterials via conventional extrusion technology. A triblock copolymer (BCP) with a cylindrical microstructure was processed via "forced assembly" to elucidate the effect of microdomain orientation on the mechanical behavior of multilayer films. The mechanical response was investigated in both the extrusion (ED) and transverse directions (TD) of the multilayer systems, revealing an influence of both cylinder-orientation and the interface on the mechanical response with decreasing layer thickness. The stress−strain curves for samples with the stress field along the cylinder axis revealed a sharp yielding phenomenon, while curves for specimens with the stress field applied perpendicular to the axis exhibited weak yielding behavior. The extensibility of the multilayer films stressed in the ED increases with decreasing layer thickness, but remains constant when deformed along the TD. Coextrusion technology allows for tunable mechanical toughness in industrial grade polymers via a continuous process. By altering the layer thickness of the two polymeric materials, we can tune the mechanics from strong, brittle behavior to a tough, ductile response by manipulation of the hierarchical structure. The enabling technology provides a unique platform to couple the inherent mechanical response of dissimilar polymers and allows for the design of composite materials with tailored mechanics.

KEYWORDS: *nanoscale organization, mechanical anisotropy, oriented block copolymers, microlayer coextrusion*

INTRODUCTION

Designing nanocomposites that are inspired by the hierarchical structures found in nature has become an important facet of the scientific community.[1] The size scale, interaction, and architecture of biological systems have been attributed to the unique behavior of materials, such as bone,[2] tendon,[3] and nacre.[4] Organization of structure from the atomistic scale to the macroscale facilitates the response of natural materials to numerous stress relief events, resulting in increased mechanical properties, such as strength and toughness.[5,6] Advanced technology in chemistry and processing, such as controlled polymerization techniques and forced assembly extrusion, have allowed design of novel materials that are inspired by nature to achieve composites with advanced structures and tunable properties.[7−12]

Processing polymers in the thin film regime has become increasingly important, as areas such as organic electronics, alternative energies, advanced membranes and biological arenas, emerge.[13] Previous research has unveiled a significant change in the physical response, such as the modulus[14] and glass transition temperature T_g,[15] of polymers when they are confined on the nanoscale.[16] Forced assembly methodologies, such as layer-by-layer assembly[17] and microlayer coextrusion,[18,19] have been used to confine polymeric materials in multilayer assemblies to probe material responses on the nanoscale.

Multilayer coextrusion is a conventional melt processing technique, where the self-assembly of polymeric materials such as block copolymers (BCPs), can be manipulated through layer reduction, affecting the physical response of the composite.[6,20−23] BCPs are easily tuned by varying their chemistry, molecular weight, volume composition, and chain architecture; they are known to self-assemble into different ordered architectures on the nanoscale, such as spherical, cylindrical,

Received: June 13, 2012
Accepted: September 5, 2012
Published: September 19, 2012

gyroid, and lamellar morphologies.[24,25] Styrenic triblock copolymers with rubbery middle blocks, such as high impact polystyrene or acrylonitrile butadiene styrene (HIPS or ABS), behave as thermoplastic elastomers (TPEs), are easily processable in the bulk state, and have improved optical transparency and resistance to thermal and chemical degradation.[26] It has been shown that the ordered microstructures of TPE BCPs have a significant impact on mechanical response (stiffness, toughness, and extensibility), suggesting a pathway toward morphology-dependent mechanical behavior.[27−30] For example, Michler has shown that, by altering the microstructure in styrenic BCPs through architecture manipulation, an increase in ductility can be achieved in materials with the same polystyrene (PS) volume composition and molecular weight.[31]

These phase-separated TPEs are an important class of elastomers due to the ability to introduce orientation within the material by an external field.[32] Electric, magnetic, and mechanical fields have been utilized to promote orientation of microdomains within a polymer matrix.[33−35] Flow fields have been shown to be advantageous over electric or magnetic fields due to the strong degree of orientation that can be introduced macroscopically; this approach is commonly used in commercial applications.[32] Keller and co-workers utilized extrusion to promote global orientation in a phase-separated BCP melt and investigate the effect of macroscale alignment on the mechanical response.[36] Further studies incorporated roll-casting[28] and reciprocating shear processing[32] to analyze the effect of BCP orientation on the deformation mechanics. Both studies revealed a high degree of mechanical anisotropy associated with the applied directional stresses in the oriented BCP systems. Roll-casting and reciprocating shear are both highly effective tools for global orientation of BCP microdomains, but are limited to batch scale production and the use of solvents in the former.

Our previous work utilized nanolayering technology to investigate the effect of confinement on the mechanical response of BCP multilayer films by systematically decreasing the layer thicknesses.[19] A cylinder-forming, styrenic BCP was coextruded between nanolayers of polystyrene (PS) in an alternating, lamellar structure and analyzed in uniaxial tension. The films were annealed to remove residual stresses of processing, and as the layer thickness decreased, the extensibility of the system increased by a factor of 12. Further investigation revealed that the PS cylinders of the BCP were aligned with the extrusion flow field, leading to a high degree of orientation within the layer thicknesses. As product design migrates toward coupling the physical properties of incompatible materials via bulk processing techniques, a detailed understanding of the microstructure assembly and the interfacial region becomes essential. In this work, our goal is to understand the effect of microstructure orientation and interfacial thickness on the deformation mechanics of confined BCPs produced via multilayer coextrusion by altering the layer thickness. It is anticipated that a material system that is mechanically anisotropic can be achieved via layer thickness manipulation by continuous melt processing of commodity polymers.

EXPERIMENTAL SECTION

Materials. Polystyrene (PS) was donated by the Dow Chemical Company, STYRON 685D (PS, Number average molecular weight, (M_n) = 128 kg/mol and polydispersity ($\overline{DP}$) = 1.60). Polystyrene-*block*-polyethylene/polypropylene-*block*-polystyrene (SEPS), a symmetric, triblock copolymer, commercially known as Kraton G1730 (M_n = 94.8 kg/mol, ($\overline{DP}$) = 1.10, styrene content ∼21% by volume and less than 1% of diblock content), was obtained from Kraton Polymers, Inc. Molecular weights were obtained by gel permeation chromatography (GPC) on a Viscotek instrument calibrated using PS standards with toluene as an eluent at a flow rate of 1 mL/min.

Processing Conditions. Multilayer films of PS and SEPS were produced via coextrusion technology described in a previous publication.[19] A 257 layer alternating system was extruded with a PS layer on both sides of the films to reduce the adhesion of the elastomer to the chill roll. The total film thickness was varied between 25 and 250 μm at a constant volume composition of 50/50, providing equal layer thicknesses of PS and SEPS. Additionally, control samples of PS and SEPS were extruded under the same conditions. The multilayer films and control specimens were annealed for 4 days under vacuum to allow sufficient reduction of residual stress built up from processing. The annealing temperature was 90 °C, which was below the glass transition temperature (T_g = 105 °C) of the PS confining layer to maintain layer integrity.

Morphological Analysis. Small-angle X-ray scattering (SAXS) measurements were conducted using a Rigaku S-MAX 3000 SAXS system. Cu Kα X-rays from a MicroMax-002+ sealed tube source (λ = 0.154 nm) were collimated through three pinhole slits to yield a final spot size of 0.7 mm at the sample position. Multilayer films were mounted in a vacuum chamber and aligned in the normal direction (ND) with respect to the X-ray beam. Two-dimensional (2D) SAXS data were collected using a Rigaku multiwire area detector with a circular active area of 133 mm and a spatial resolution of 1024 × 1024 pixels. The sample-to-detector distance and the scattering vector, q, were calibrated using a silver behenate (AgBe) standard with a characteristic (001) peak position at q = 1.076 nm^{-1}. The calculated sample-to-detector distance was 1.5 m. Typical exposure times for ND SAXS patterns were collected for 3 h because of low scattering intensity from the SEPS. All X-ray images were processed using software named "POLAR" (Stonybrook Technology and Applied Research, Inc.).

Scanning electron microscopy (SEM) was utilized to investigate the deformation mechanics of the multilayer films. The deformed samples were embedded in a 5 min epoxy and allowed to cure overnight. After curing, the samples were cryotomed perpendicular to the deformation axis to analyze the edge-on view at a cutting temperature of −70 °C with a glass knife temperature of −60 °C. The samples were then sputter coated in gold and analyzed on a JEOL JSM-6510LV SEM at a voltage of 15 kV.

Uniaxial Mechanical Analysis. Uniaxial tensile deformation was performed on an Instron mechanical testing instrument at room temperature with a 1 kN load cell. The samples were cut in both the extrusion and transverse directions with a steel die according to ASTM D638 with a minimum of five samples per layer thickness. The PS/SEPS multilayer films were elongated at room temperature under a constant strain rate of 10% strain per minute.

RESULTS AND DISCUSSION

Forced-assembly coextrusion was utilized to produce alternating multilayer films of PS and SEPS at equal volume compositions (50 vol%/50 vol%).[19] PS was processed on both surfaces of the multilayer films to provide maximum confinement of the elastomeric BCP and reduce adhesion to the chill roll. Additionally, the control samples, PS and SEPS, and the multilayer films were annealed under vacuum to relieve stress build-up from the extrusion process.

Orientation of PS Cylinders in PS/SEPS Multilayer Films. Morphological studies of the annealed samples previously indicated that the styrenic cylinders of the BCP became highly oriented as the layers approach 100 nm, while a more isotropic arrangement of the cylinders were observed in the thicker nanolayers.[19] The high degree of orientation was attributed to flow-induced alignment resulting from the

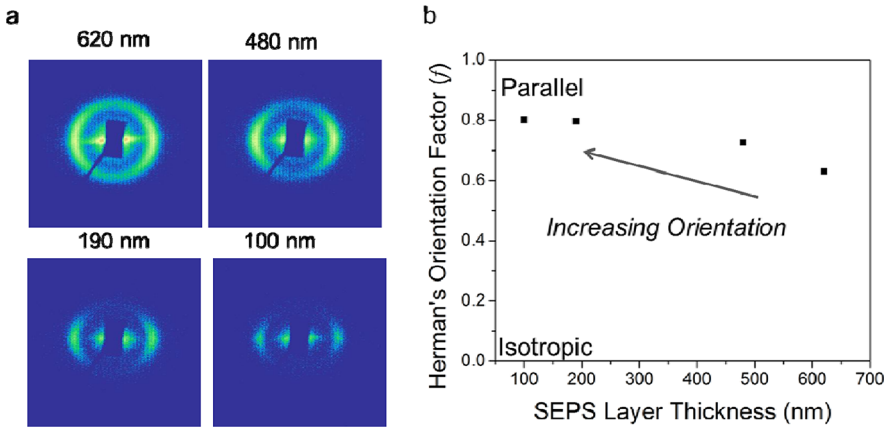

Figure 1. (a) 2D SAXS scattering patterns for PS/SEPS multilayer films (see the Supporting Information).[19] Reprinted with permission from ref 19. Copyright 2012 American Chemical Society. (b) Effect of layer thickness on the Herman's orientation factor.

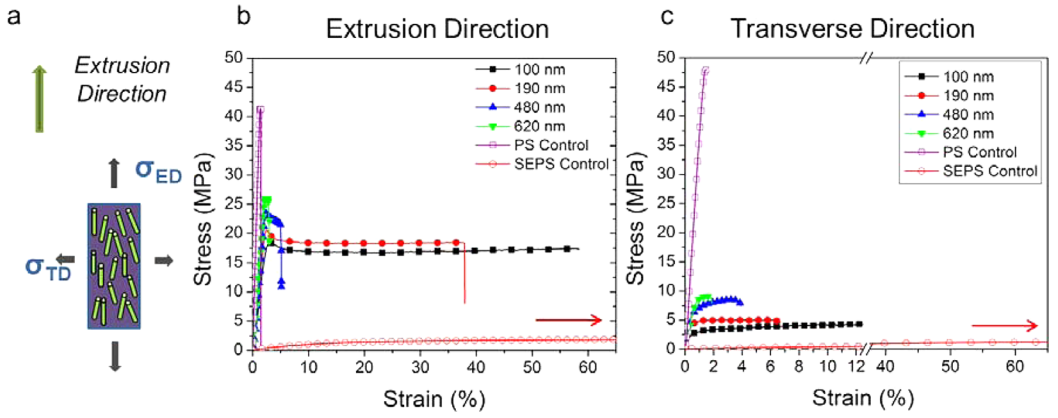

Figure 2. (a) Schematic representation of stress field orientations. Stress−strain response of annealed PS/SEPS multilayer films. (b) Extrusion direction. Reprinted with permission from ref 19. Copyright 2012 American Chemical Society. (c) Transverse direction.

extrusion process. Information regarding the degree of orientation of the PS cylinders was obtained by integrating the azimuthal angles, χ, from 0° to 180° for the multilayer films. Similar calculations have been shown for liquid crystalline materials with respect to the director as the order parameter.[37] In this research, the Herman's orientation factor, analogous to the order parameter, was used to analyze the degree of orientation as a function of layer thickness

$$F = C^{-1}(3\langle\cos^2\chi\rangle - 1)/2$$

where, χ, is the azimuthal angle, $\langle\cos^2\chi\rangle$ is the average of $\cos^2\chi$ from the equation

$$\langle\cos^2\chi\rangle = \frac{\int_0^\pi I(\theta,\chi)\cos^2(\chi)\sin(\chi)\mathrm{d}\chi}{\int_0^\pi I(\theta,\chi)\sin(\chi)\mathrm{d}\chi}$$

and the scattered intensity at the polar (θ) and azimuthal (χ) angles are represented by $I(\theta,\chi)$. C is a conversion constant for cylinder orientation normal to the stretching direction and is −1/2 when the angle is 90°.[38] The orientation factor for an oriented cylindrical system is 1, while an isotropic system is 0. It was observed that, as the layer thickness decreased, the PS cylinders became highly oriented, resulting in an increase in the orientation factor (Figure 1). The 2D SAXS scattering patterns show a narrowing of the arcs at the equator as a function of layer thickness, which was attributed to the confinement of the BCP by the PS layer and subsequent restriction of the rearrangement of the cylinders with postprocessing heat treatment.

Deformation Study of PS/SEPS Multilayer Films. Research pioneered by Keller and co-workers[36,39] revealed that highly oriented, cylinder-forming BCPs exhibit an anisotropic mechanical response in the small strain regime that was later correlated to the deformation mechanics of the cylinder microstructure by Thomas et al.[32,40] However, in these studies the BCP has a low modulus because of its elastomeric nature. In this research, we explored the mechanical properties of multilayer films that couple the mechanical response of a high modulus material and a phase-separated BCP. Tensile samples were evaluated from the multilayer films in both the extrusion direction (ED), which is parallel to the longitudinal axis of the cylinder, and the transverse direction (TD), which is perpendicular to the cylinder axis (Figure 2a). The mechanical properties for each layer thickness in the TD are tabulated in Table S1. The ED mechanical data was previously reported.[19]

Elastic Modulus. The elastic modulus of alternating lamellar composites has been routinely characterized by the Voigt average model, which considers the modulus and volume fraction of each material component.[41] This simple model does not account for the orientation factor of the BCP as the filler phase. Previous research by Odell and Keller revealed that the axial modulus (parallel to cylinder axis) of oriented BCP microdomains was drastically higher than that of isotropic BCPs and 100x higher than the transverse moduli values.[36,39]

dx.doi.org/10.1021/am301072s | ACS Appl. Mater. Interfaces 2012, 4, 5155−5161

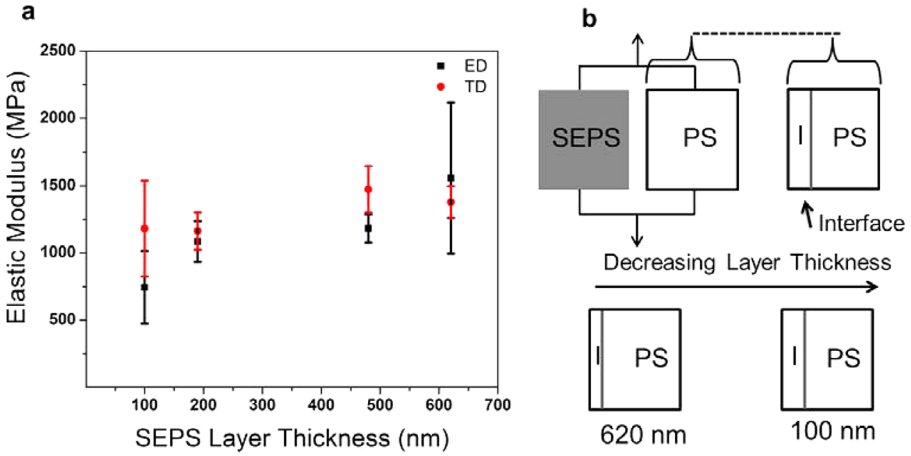

Figure 3. (a) Effect of layer thickness on the elastic modulus of PS/SEPS multilayer films. (b) Schematic representation of composite model (3 components, PS, SEPS, and I-interphase).

On the basis of this study, we initially anticipated an increase in the bulk modulus with decreasing layer thickness. However, further investigation revealed a loss in overall mechanical response with increasing BCP orientation (e.g., decreasing layer thickness) in both the ED and TD (Figure 3a). We postulated that this observed response was attributed to contributions from the interphase region. Previous studies have shown that, as the thickness of a homopolymer PS film decreases, the resulting modulus decreases due to an expansion in free volume.[14,42] In the PS/SEPS multilayer system, it would be expected that a wetting layer of the lower molecular weight PS end blocks in SEPS swell the interfacial region of the PS layers, resulting in a material with a decreased modulus. The theoretical interphase thickness from the thermodynamic interaction parameter was calculated using the following equation[43]

$$d_I = \frac{2b}{(6\chi)^{0.5}}$$

where b is the statistical segment step length and is taken as 6.7 and 6.07 Å for PS and SEPS, respectively.[44] The Flory–Huggins interaction parameter is estimated from the solubility parameters, δ_i, of the extruded polymers given by the equation

$$\chi = \frac{V}{RT}(\delta_{PS} - \delta_{SEPS})^2$$

where V is the molar volume taken at the processing temperature, δ_{PS} is 17.52 $MPa^{1/2}$, and δ_{SEPS} is 17.29 $MPa^{1/2}$.[45] The calculated interphase thickness was determined to be 13.02 nm for the multilayer films of PS and SEPS, which is comparable to length scales observed via TEM (Supporting Information, Figure S1). This interfacial region results from the wetting layer created by the swelling of the PS layer by the short PS end blocks in the SEPS layer, which becomes significant fraction (10.5 vol %) as the multilayer film thickness decreases. As the total thickness of the films decreases from 200 to 25 μm, the effective volume fraction of the interphase increases from around 1.67% of the total film thickness in the thicker PS layers to almost 14% of the total film thickness in the 100 nm layer films (Figure 3b), resulting in a decrease in the effective PS layer thickness. We assumed a linear, gradient modulus for the interface to calculate the total composite modulus based on volume composition (Table 1). As a result, the PS layer modulus was reduced, which corresponded to a decrease in the calculated total composite modulus. These calculated composite modulus values followed a trend similar to the experimental stress–strain curves (Figure 3a) in both the ED and TD for the multilayer films (i.e., decreasing modulus with decreasing layer thickness). These results indicate that the modulus of the interface has a stronger effect on the overall composite modulus than the modulus of the oriented PS cylinders.

Table 1. Calculated Mechanical Properties of PS/SEPS Multilayer Films As a Function of Interphase Thickness

PS/SEPS film thickness (μm)	PS layer thickness (nm)	interface thickness (%)	calculated PS layer modulus (MPa)	calculated composite modulus (MPa)
200	620	1.67	2970	1490
125	480	2.67	2970	1480
50	190	6.66	2920	1430
25	100	13.3	2840	1340

Yield Stress. The shape of the stress–strain curves in the yielding region varied depending upon the orientation of the deformation stress to the extrusion direction. The samples cut in the extrusion direction exhibited a high yield stress and a resulting abrupt yield point. Beyond the yield point, the stress level was maintained for all films tested parallel to the cylinder axis irrespective of layer thickness (Figure 2b). However, the mechanical response in the transverse direction resulted in a weak yielding phenomenon that led to brittle fracture with minimal elasticity (Figure 2c). The samples in the TD failed prior to establishing a proper yield point, so the yield stress was calculated from the intersection of tangential lines of the modulus and plateau yield stress. We observed that the direction of the deformation stress has a significant effect on the shape of the stress–strain curve and resulting yield stress, but the yield stress changes very little with layer thickness, approximately ±2 MPa. In our multilayer films, the yield stress in the ED was 4x higher than in the TD (Figure 4a), which was correlated to the stress required to deform the PS cylinders as reported previously by Thomas et al.[46] When stress is applied along the longitudinal axis of the cylinders, the PS cylinders are elongated, allowing the BCP to reach a higher yield stress and then fracture into smaller PS fragments. The fractured PS microdomains act as spherical reinforcing agents and maintain a high level of stress post-yielding. In contrast, when the stress is

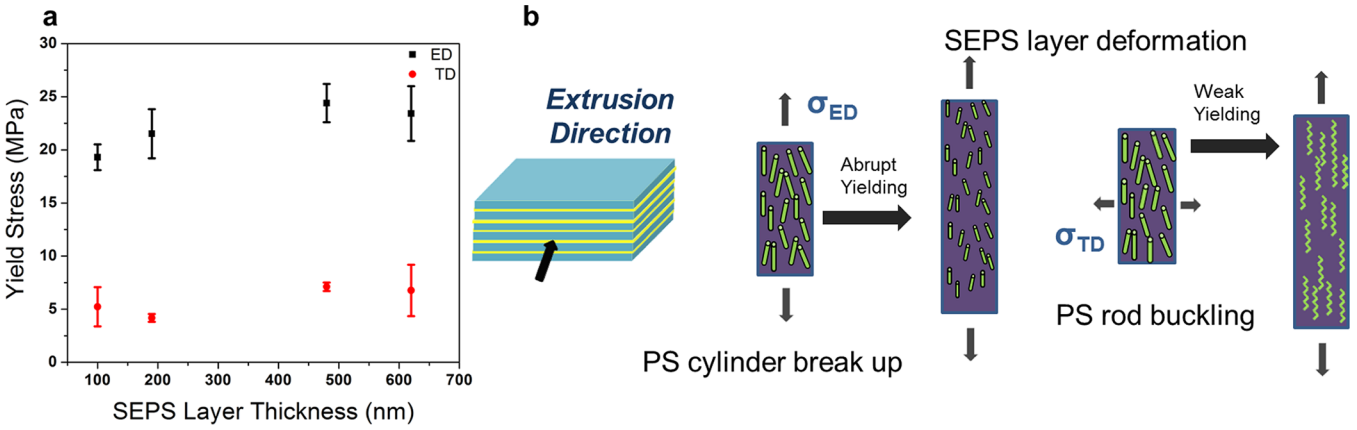

Figure 4. (a) Effect of layer thickness on the yield stress of PS/SEPS multilayer films. (b) Schematic representation of the deformation of PS microdomains.

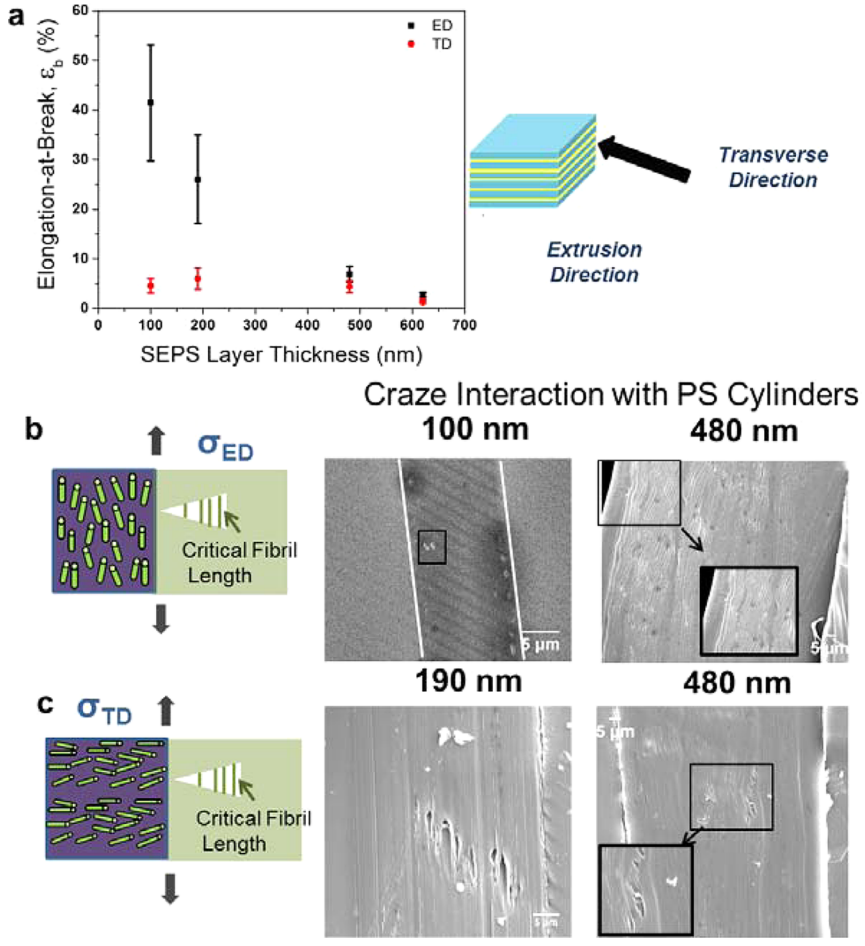

Figure 5. (a) Effect of layer thickness on the elongation-at-break of PS/SEPS multilayer films. (b) Schematic and micrographs of craze propagation in the extrusion direction. (c) Schematic and micrographs of craze propagation in the transverse direction. Boxed images enlarged for detail.

applied in the transverse direction, the load is carried by the elastomeric matrix, pulling the adjacent cylinders apart and leading to the formation of a chevron-pattern PS phase as reported by Tarasov until fracture (Figure 4b).[47]

Elongation-at-Break (ε_b). Beyond the yield point of the stress−strain curves, the extensibility of the multilayer films also exhibited an anisotropic response (Figure 5a). In the ED, the elongation-at-break increased exponentially with decreasing layer thickness and increasing BCP domain orientation (black points). When the multilayer films were analyzed in the TD, we observed no layer dependence on the fracture strain (red points). These results indicated that there is a significant effect on the plastic deformation mechanism as a function of microstructure orientation. We attribute this anisotropy to thin-layer yielding, where craze fronts are blunted allowing the polymer to reach higher strains. Similar increases in ductility have been observed in homopolymer and multilayer films as well as in BCP systems.[48−50] These results are indicative of two

dx.doi.org/10.1021/am301072s | ACS Appl. Mater. Interfaces 2012, 4, 5155−5161

modes of plastic deformation, resulting in either crazing or shear yielding. Upon loading in the extrusion direction, the craze front propagated perpendicular to the longitudinal axis of the cylinders in the thin layers, which restricted the formation of cracks and resulted in a controlled stress relief event across the film (Figure 5b). This mechanism was supported by shear yielding and a necking region, which remains transparent in films with layer thickness less than 200 nm. In contrast, the thicker layers exhibited stress whitening from craze formation, which occurred due to the more isotropic nature of the cylinders (Figure 5b). To confirm these proposed deformation mechanisms in the extrusion direction, SEM and SAXS were utilized to confirm the presence of crazes in the thick layers of the deformed samples. Significant voiding and a large damage zone near the failure region were observed in the thicker, 480 nm layers, which is indicative of crazing. In the thin, 100 nm layers, there is no significant sign of voiding in the deformation zone that would suggest the presence of crazes.[51] Microvoids were observed near the edge of the thin film, which was attributed to delamination between the film and the epoxy. In the transverse direction, the craze fronts propagated parallel to the cylinder axis, allowing craze fibrils to reach a critical length that lead to ultimate failure (Figure 5c).[52] Stress whitening was observed in all layer thicknesses deformed in the TD, indicating crazes propagating to cracks.[53,54] The SEM images of the deformed samples confirmed the formation of microvoids in both the thin (190 nm) and thick (480 nm) films. Large void regions are indicative of brittle failure through a crazing mechanism. Similar voiding has been previously imaged in multilayer films for dielectrics, resulting from crazing as the breakdown mechanism.[51] In conjunction with SEM, SAXS was conducted on the deformed multilayer films in both the ED (Supporting Information Figure S2) and TD (Supporting Information Figure S3). SAXS analysis revealed a characteristic scattering vector peak of 0.26 nm^{-1}. from craze fibrils[55,56] in all of the samples except the 100 nm ED, which was in agreement with the SEM images. Previous research has shown that this scattering vector correlates to the length scale between the fibrils spanning the craze.[57] A detailed experimental procedure is outlined in the Supporting Information to confirm the observed deformation mechanics.

Toughness. Mechanical toughness is defined as the amount of energy a material can absorb measured as the area under the stress−strain curve. The ability to influence the shape of the stress−strain curve via confined BCP orientation and layer thickness allows for the development of a material system with tunable overall toughness. In our multilayer systems, the observed toughness enhancement was a result of a combination of thin PS layers, which become more extensible as layer thicknesses decrease and result in a brittle-to-ductile transition in the multilayer films, and the orientation of the BCP, which allows for a tunable yield stress (Figure 6). As a result of the hierarchical structure developed via forced assembly, a material with tailored mechanical toughness can be fabricated via systematic changes in layer thickness and degree of orientation.

CONCLUSIONS

In this research, the mechanical properties of a multilayer system of PS and SEPS were examined by applying a uniaxial stress along the extrusion and transverse directions to the axis of cylinder alignment. It was shown that the material response is dependent upon the orientation of the BCP microstructures and influenced by the interphase region as a function of layer thickness. The resulting anisotropy can be attributed to the failure of the PS cylinders within the block copolymer with increasing degree of alignment to the applied force, resulting in variations in yielding phenomena. Further investigation revealed an increase in material toughness because of a combination of deformation of thin film PS in direct contact with an elastomeric material, and orientation of PS microstructure within the film plane, which allows access to the brittle-to-ductile transition. We have demonstrated the ability to combine self-assembly and forced assembly, allowing for the development of hierarchical structures with tunable mechanical response in a bulk material process. The ability to acquire tunable mechanical properties from a continuous extrusion process through interface and orientation manipulation is advantageous for industrial processing flexibility.

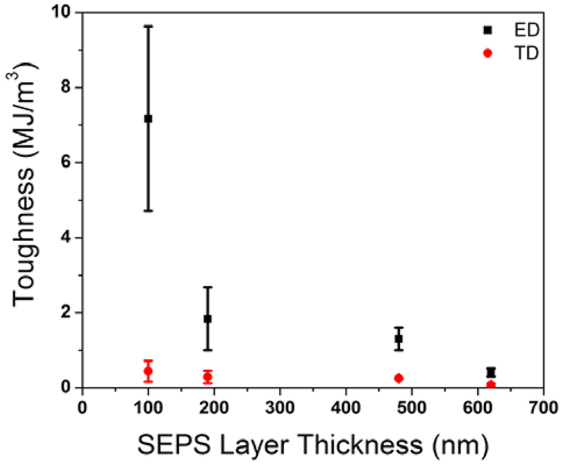

Figure 6. Effect of layer thickness on the toughness of PS/SEPS multilayer films.

ASSOCIATED CONTENT

Supporting Information

Transmission electron microscopy images (TEM), mechanical properties table and small-angle X-ray scattering (SAXS) plots are available free of charge via the Internet at http://pubs.acs.org.

AUTHOR INFORMATION

Corresponding Author

*Phone: (216) 368-1421. E-mail: ltk13@case.edu.

Notes

The authors declare no competing financial interest.

ACKNOWLEDGMENTS

This research was supported by the NSF Science and Technology Center through the Center for Layered Polymeric Systems, CLiPS under Grant 0423914. The authors would also like to Nandula Wanasekara and Seyedali Monemian for the assistance with SEM and TEM, respectively, and Prof. Eric Baer for discussions on failure mechanics.

REFERENCES

(1) Stone, D. A.; Korley, L. T. J. *Macromolecules* **2010**, *43*, 9217−9226.
(2) Fratzl, P. *Nat. Mater.* **2008**, *7*, 610−612.
(3) Kastelic, J.; Baer, E. *Symp. Soc. Exp. Biol.* **1980**, *34*, 397−435.

(4) Smith, B. L.; Schaffer, T. E.; Viani, M.; Thompson, J. B.; Frederick, N. A.; Kindt, J.; Belcher, A.; Stucky, G. D.; Morse, D. E.; Hansma, P. K. *Nature* **1999**, *399*, 761−763.
(5) Tirrell, D. A.; Aksay, I.; Baer, E.; Calvert, P. D.; Cappello, J.; Dimarzio, E. A.; Evans, E. A.; Fessler, J.; Wainwright, S. A. *Hierarchical structures in biology as a guide for new materials technology*; National Research Council; National Academy Press: Washington, D.C., 1994.
(6) Baer, E.; Hiltner, A.; Jarus, D. *Macromol. Symp.* **1999**, *147*, 37−61.
(7) Fox, J. D.; Rowan, S. J. *Macromolecules* **2009**, *42*, 6823−6835.
(8) Shanmuganathan, K.; Capadona, J. R.; Rowan, S. J.; Weder, C. *Prog. Polym. Sci.* **2010**, *35*, 212−222.
(9) Stone, D. A.; Wanasekara, N. D.; Jones, D. H.; Wheeler, N. R.; Wilusz, E.; Zukas, W.; Wnek, G. E.; Korley, L. T. J. *ACS Macro Lett.* **2011**, *1*, 80−83.
(10) Stone, D. A.; Hsu, L.; Wheeler, N. R.; Wilusz, E.; Zukas, W.; Wnek, G. E.; Korley, L. T. J. *Soft Matter* **2011**, 7.
(11) Stone, D. A.; Wanasekara, N. D.; Jones, D. H.; Wheeler, N. R.; Wilusz, E.; Zukas, W.; Wnek, G. E.; Korley, L. T. J. *ACS Macro Lett.* **2011**, *1*, 80−83.
(12) Johnson, J. C.; Wanasekara, N. D.; Korley, L. T. J. *Biomacromolecules* **2012**, *13*, 1279−1286.
(13) Lee, J.-H.; Chung, J. Y.; Stafford, C. M. *ACS Macro Lett.* **2011**, *1*, 122−126.
(14) Stafford, C. M.; Vogt, B. D.; Harrison, C.; Julthongpiput, D.; Huang, R. *Macromolecules* **2006**, *39*, 5095−5099.
(15) Kim, S.; Roth, C. B.; Torkelson, J. M. *J. Polym. Sci. Pol. Phys.* **2008**, *46*, 2754−2764.
(16) Alcoutlabi, M.; McKenna, G. B. *J. Phys.:Condens. Matter* **2005**, *17*, R461−R524.
(17) Hammond, P. T. *Adv. Mater.* **2004**, *16*, 1271−1293.
(18) Carr, J. M.; Langhe, D. S.; Langhe, Ponting, M. T.; Hiltner, A.; Baer, E. *J. Mater. Res.* **2012**, *27*, 1326.
(19) Burt, T. M.; Keum, J.; Hiltner, A.; Baer, E.; Korley, L. T. J. *ACS Appl. Mater. Interfaces* **2011**, *3*, 4804−4811.
(20) Tangirala, R.; Baer, E.; Hiltner, A.; Weder, C. *Adv. Funct. Mater.* **2004**, *14*, 595−604.
(21) Ranade, A. P.; Hiltner, A.; Baer, E.; Bland, D. G. *J. Cell. Plast.* **2004**, *40*, 497−507.
(22) Kazmierczak, T.; Song, H. M.; Hiltner, A.; Baer, E. *Macromol. Rapid Commun.* **2007**, *28*, 2210−2216.
(23) Pethe, V. V.; Wang, H. P.; Hiltner, A.; Baer, E.; Freeman, B. D. *J. Appl. Polym. Sci.* **2008**, *110*, 1411−1419.
(24) Hamley, I. *The Physics of Block Copolymers*; Oxford Science Publications: Oxford, U.K., 1998.
(25) Bates, F. S.; Fredrickson, G. H. *Annu. Rev. Phys. Chem.* **1990**, *41*, 525−557.
(26) Spontak, R. J.; Patel, N. P. *Curr. Opin. Colloid Interface Sci.* **2000**, *5*, 334−341.
(27) Mahanthappa, M. K.; Lim, L. S.; Hillmyer, M. A.; Bates, F. S. *Macromolecules* **2007**, *40*, 1585−1593.
(28) Mahanthappa, M. K.; Hillmyer, M. A.; Bates, F. S. *Macromolecules* **2008**, *41*, 1341−1351.
(29) Mamodia, M.; Indukuri, K.; Atkins, E. T.; De Jeu, W. H.; Lesser, A. *J. Mater. Sci.* **2008**, *43*, 7035−7046.
(30) Huy, T. A.; Adhikari, R.; Michler, G. H. *Polymer* **2003**, *44*, 1247−1257.
(31) Adhikari, R.; Michler, G. H.; Huy, T. A.; Ivan'kova, E.; Godehardt, R.; Lebek, W.; Knoll, K. *Macromol. Chem. Phys.* **2003**, *204*, 488−499.
(32) Honeker, C. C.; Thomas, E. L. *Chem. Mater.* **1996**, *8*, 1702−1714.
(33) Amundson, K.; Helfand, E.; Quan, X.; Smith, S. D. *Macromolecules* **1993**, *26*, 2698−2703.
(34) Amundson, K.; Helfand, E.; Quan, X. N.; Hudson, S. D.; Smith, S. D. *Macromolecules* **1994**, *27*, 6559−6570.
(35) Larson, R. G. *Rheol. Acta* **1992**, *31*, 497−520.
(36) Odell, J. A.; Arridge, R. G. C.; Folkes, M. J.; Keller, A. *Abstr. Pap. Am. Chem. Soc.* **1977**, *173*, 27−27.
(37) Alger, M. S. M. *Polymer Science Dictionary*, 2nd ed.; Champan & Hall: London, 1997; pp 352−353.
(38) Stasiak, J.; Squires, A. M.; Castelletto, V.; Hamley, I. W.; Moggridge, G. D. *Macromolecules* **2009**, *42*, 5256−5265.
(39) Arridge, R. G. C.; Folkes, M. J. *J. Phys. D: Appl. Phys.* **1972**, *5*, 344.
(40) Honeker, C. C.; Thomas, E. L.; Albalak, R. J.; Hajduk, D. A.; Gruner, S. M.; Capel, M. C. *Macromolecules* **2000**, *33*, 9395−9406.
(41) Verbeek, C. J. R.; Focke, W. W. *Composites, Part A* **2002**, *33*, 1697−1704.
(42) Vandersanden, M. C. M.; Meijer, H. E. H.; Lemstra, P. J. *Polymer* **1993**, *34*, 2148−2154.
(43) Liu, R. Y. F.; Bernal-Lara, T. E.; Hiltner, A.; Baer, E. *Macromolecules* **2004**, *37*, 6972−6979.
(44) Fetters, L. J.; Lohse, D. J.; Richter, D.; Witten, T. A.; Zirkel, A. *Macromolecules* **1994**, *27*, 4639−4647.
(45) Ahmad, H.; Yaseen, M. *Polym. Eng. Sci.* **1979**, *19*, 858−863.
(46) Villar, M. A.; Rueda, D. R.; Ania, F.; Thomas, E. L. *Polymer* **2002**, *43*, 5139−5145.
(47) Tarasov, S. G.; Tsvankin, D. Y.; Godovskii, Y. K. *Vysokomol. Soedin., Ser. A* **1978**, *20*, 1534.
(48) Adhikari, R.; Lach, R.; Michler, G. H.; Weidisch, R.; Knoll, K. *Macromol. Mater. Eng.* **2003**, *288*, 432−439.
(49) Kerns, J.; Hsieh, A.; Hiltner, A.; Baer, E. *Macromol. Symp.* **1999**, *147*, 15−25.
(50) Argon, A. S.; Cohen, R. E.; Gebizlioglu, O. S.; Brown, H. R.; Kramer, E. J. *Macromolecules* **1990**, *23*, 3975−3982.
(51) Mackey, M.; Hiltner, A.; Baer, E.; Flandin, L.; Wolak, M. A.; Shirk, J. S. *J. Phys. D: Appl. Phys.* **2009**, 42.
(52) Ruokolainen, J.; Fredrickson, G. H.; Kramer, E. J.; Ryu, C. Y.; Hahn, S. F.; Magonov, S. N. *Macromolecules* **2002**, *35*, 9391−9402.
(53) Donald, A. M.; Kramer, E. J. *J. Mater. Sci.* **1982**, *17*, 1765−1772.
(54) Jang, B. Z.; Uhlmann, D. R.; Sande, J. B. V. *J. Appl. Polym. Sci.* **1984**, *29*, 3409−3420.
(55) Renouf-Glauser, A. C.; Rose, J.; Farrar, D.; Cameron, R. E. *Biomaterials* **2005**, *26*, 2415−2422.
(56) Brown, H. R.; Kramer, E. J. *J. Macromol. Sci., Part B:Phys.* **1981**, *19*, 487−522.
(57) Magalhaes, A. M. L.; Borggreve, R. J. M. *Macromolecules* **1995**, *28*, 5841−5851.